Magnetic Field Effect on Multiplicity of Solutions Induced by Thermosolutal Convection in a Bénard Square Porous Cavity Submitted to Horizontal Concentration Gradient

A. Mansour†, M. Ait Ahmed, A. Amahmid, M. Hasnaoui, I. Filahi and Y. Dahani

Cadi Ayyad University, Faculty of Sciences Semlalia, Department of Physics,
LMFE, BP 2390 Marrakesh, Morocco

†*Corresponding Author Email: a.mansour@uca.ma*

ABSTRACT

In this work, we present a numerical study of the magnetic field effect on double diffusive natural convection in a square porous cavity saturated with an electrically conducting binary mixture. The cavity is heated from below and cooled from the top, while its vertical walls are adiabatic and maintained at constant but different concentrations. The numerical results are obtained for a Lewis number $Le = 10$ and the following ranges for the other controlling parameters: $40 \leq R_T \leq 1000$, $-0.2 \leq N \leq 0.2$ and $-0.5 \leq Ha \leq 0.5$, where R_T, N and Ha are the thermal Rayleigh number, the buoyancy ratio and the Hartmann parameter, respectively. First, the effect of the Hartmann parameter on the maintenance and disappearance of the multiple steady state solutions obtained in the case of purely thermal convection is examined. Then, the combined effect of N and Ha on the existence of these steady solutions is analyzed. It is found that the critical values of N corresponding to the transitions between the different solutions are modified by the application of a magnetic field. However, the nature of the transitions is unchanged. It is shown that the magnetic field may affect considerably the flow intensity and the heat and mass transfer in the medium.

NOMENCLATURE

B_0	strength of the magnetic field	T_c'	dimensional temperature at the upper horizontal wall of the cavity
BF	Bicellular Flow		
BAF	Bicellular Anti-natural Flow	T_h'	dimensional temperature at the lower horizontal wall of the cavity
BNF	Bicellular Natural Flow		
D	mass diffusivity	$\Delta T'$	temperature difference
Ha	Hartmann number	(u, v)	dimensionless velocities in (x, y) directions
g	gravitational acceleration		
K	permeability of the porous medium	(x, y)	dimensionless coordinates
L'	length of the porous cavity	α	thermal diffusivity
Le	Lewis number	β_S	solutal expansion coefficient
MF	Monocellular Flow	β_T	thermal expansion coefficient
MCF	Monocellular Clockwise Flow	ε	normalized porosity
MTF	Monocellular Trigonometric Flow	ε'	porosity of the porous medium
N	buoyancy ratio	λ	thermal conductivity of the saturated porous medium
Nu	Nusselt number		
R_T	thermal Rayleigh number	ν	kinematic viscosity of the fluid
S	dimensionless concentration	μ	dynamic viscosity of the fluid
S_0'	dimensional concentration of the left wall	ϵ	electrical conductivity of the fluid
S_1'	dimensional concentration of the right wall	ρ	density of the fluid mixture
Sh	Sherwood number	$(\rho c)_f$	heat capacity of the fluid mixture
$\Delta S'$	concentration difference	$(\rho c)_p$	heat capacity of the saturated porous

t	dimensionless time		medium
T	dimensionless temperature	σ	heat capacity ratio
TCF	tricellular flow with a clockwise central cell	Ψ	dimensionless stream function
TF	tricellular flow		
TTF	tricellular flow with a trigonometric central cell		

Subscripts
cr   critical value
ext   extremum value
max   maximum value

Superscripts
′   dimensional variable

1. INTRODUCTION

The magnetic field is a good control parameter on heat transfer and fluid flow and is also used to reach maximum efficiency in thermodynamics in different fields (Kabeel *et al.* 2015; Kasaeian *et al.* 2017). The problem of natural convection in an electrically conducting fluid under a magnetic field has been the subject of numerous studies (Hussein *et al.* 2014; Bahiraei and Hangi 2015). This interest stems from the implication of the phenomenon in many engineering applications such as crystal growth processes.

Several researchers have studied the effect of the magnetic field on pure thermal convection. Here we cannot quote all these works but we will present some investigations. In fact, the influence of a uniform magnetic field on natural convection in square cavity was studied by Krakov and Nikiforov (2002). They discovered that the angle between the direction of the temperature gradient and magnetic field influences the convective structure and the heat flux. Sophy *et al.* (2005) studied the thermomagnetic convection in a differentially heated square cavity. These authors showed that the flow pattern underwent a great modification when the maximum value of the magnetic field was beyond a critical threshold and heat exchange at the walls increases. Zeng *et al.* (2007) studied numerically natural convection in an enclosure filled with a fluid-saturated porous medium and submitted to a strong magnetic field. Two physical configurations were considered by these authors. The first one was heated from the bottom and cooled from the top, and the second was heated from the left side vertical wall and cooled from the opposite wall. An electric coil was set below this enclosure to generate a magnetic field. A numerical investigation for penetrative ferroconvection via internal heat generation in a ferrofluid saturated porous layer was performed by Nanjundappa *et al.* (2012). Heidary *et al.* (2016) analyzed natural convection in porous inclined enclosures, equipped with one or two obstacles, with the presence of sinusoidal heated wall and magnetic field. Hoshyar *et al.* (2016) showed that the Least Square Method (LSM) is a powerful and easy-to-use analytic tool for predicting the temperature distribution in a porous fin which was exposed to uniform magnetic field. An experimental study of heat transfer enhancement due to laminar ferrofluid flow in a horizontal tube partially filled with porous media under fixed parallel magnet bars was carried out by Sheikhnejad *et al.* (2017). In this study, it was found that the presence of both porous media and magnetic field simultaneously could highly improve heat transfer. The impact of an external magnetic field on the hydrothermal aspects of natural convection of a power-law non-Newtonian nanofluid inside a baffled U-shaped enclosure was examined by Ali *et al.* (2020). They reported that the cooling performance of a cavity augments with the rise of aspect ratio, nanoparticle volume fraction, Rayleigh number, while it is reduced by boosting the Hartmann number.

On another side, many efforts have been devoted by the researchers to understand the effect of magnetic field on double diffusion. In this frame, Chamkha and Al-Naser (2002) studied numerically the characteristics of hydromagnetic double-diffusive convective flow of a binary gas mixture in a rectangular enclosure with the upper and lower walls being insulated, while constant temperatures and concentrations are imposed along the left and right walls. A uniform magnetic field was applied in the x-direction. The same authors conducted a similar study by imposing heat and mass fluxes on the vertical walls (2002). Robillard *et al.* (2006) studied analytically and numerically the electromagnetic field effect on the natural convection in a vertical porous cavity saturated with an electrically conducting binary mixture. An analytical and numerical investigation was conducted by Ramambason and Vasseur (2007) to study the effect of an electromagnetic filed on natural convection in a horizontal shallow porous cavity filled with an electrically conducting binary mixture. A uniform heat flux was applied on the horizontal walls of the layer while the vertical walls were adiabatic. Numerical simulation of double-diffusive natural convective flow in an inclined rectangular enclosure in the presence of magnetic field and heat source was conducted by Teamah *et al.* (2012). The effect of magnetic field on 3D double diffusive convection in a cubic cavity filled with a binary mixture was considered by Maatki *et al.* (2013). The influence of the magnetic field on the structure of the three-dimensional flow, the distribution of temperature and concentration and the different characteristics of heat and mass transfer of the thermal and solutal dominated region were presented. Teamah *et al.* (2016) investigated the magnetic field effect on double diffusive convection in a trapezoidal enclosure.

In this investigation, the attention is focused on the magnetic field effect on the multiple steady state solutions induced in a square porous cavity saturated with an electrically conducting binary mixture. The cavity is heated from below and cooled from the top, while its vertical walls are adiabatic and maintained at constant but different concentrations. This configuration was considered in the past by Altawalbeh *et al.* (2013) without taking into account the multiplicity of solutions generated for adequate ranges of the governing parameters. Our objective in this work is to examine the influence of the magnetic field on the existence range of different types of steady-state solutions. Results for heat and mass transfer induced by these solutions are also presented and discussed. Note that in previous studies conducted by Robillad *et al.* (1998), Bourich *et al.* (2004) and Mansour *et al.* (2006), it was shown that these quantities may be considerably affected by the type of solution.

2. MATHEMATICAL FORMULATION

The system under consideration (Fig. 1) is a square cavity filled with an isotropic and homogenous porous medium, saturated with an electrically conducting binary mixture. The bottom wall of the cavity is maintained at a hot temperature T_h', while the top one is maintained at a cold temperature T_c'. The right vertical wall is maintained at a concentration (S_1') higher than that of the left one (S_0'). The top and bottom walls are assumed impermeable to mass transfer, while the right and left ones are assumed adiabatic. A magnetic field of strength B_0 is applied in a direction normal to the horizontal walls of the porous cavity. The thermophysical properties of the binary fluid are considered constant except the density in the buoyancy term which varies linearly with the local temperature and concentration (Boussinesq approximation):

$$\rho = \rho_0 \left[1 - \beta_T \left(T' - T_0' \right) - \beta_S \left(S' - S_0' \right) \right]$$

where β_T and β_S are, respectively, the thermal and solutal expansion coefficients of the binary fluid, T' is the dimensional temperature and S' is the concentration (T_0' and S_0' correspond to the reference state). Viscous dissipation is neglected and the solid matrix and the fluid are assumed to be at local thermal equilibrium. Using the Darcy model and taking into account the magnetic field effect, the dimensionless equations governing the flow and heat and mass transfer in the saturated porous medium are written as follows:
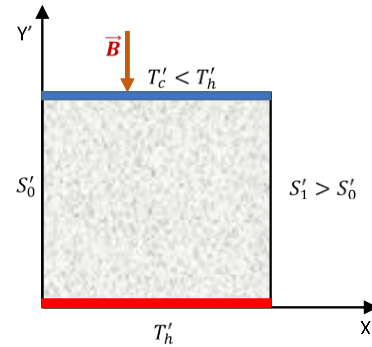
$$\frac{\partial^2 \boldsymbol{\Psi}}{\partial^2 \boldsymbol{X}} + \left(1 + \boldsymbol{Ha}^2 \right) \frac{\partial^2 \boldsymbol{\Psi}}{\partial^2 \boldsymbol{Y}} = -\boldsymbol{R_T} \left(\frac{\partial \boldsymbol{T}}{\partial \boldsymbol{X}} + \boldsymbol{N} \frac{\partial \boldsymbol{S}}{\partial \boldsymbol{X}} \right) \quad (1)$$

$$\frac{\partial \boldsymbol{T}}{\partial \boldsymbol{t}} + \boldsymbol{U} \frac{\partial \boldsymbol{T}}{\partial \boldsymbol{X}} + \boldsymbol{V} \frac{\partial \boldsymbol{T}}{\partial \boldsymbol{Y}} = \nabla^2 \boldsymbol{T} \quad (2)$$

$$\varepsilon \frac{\partial \boldsymbol{S}}{\partial \boldsymbol{t}} + \boldsymbol{U} \frac{\partial \boldsymbol{S}}{\partial \boldsymbol{X}} + \boldsymbol{V} \frac{\partial \boldsymbol{S}}{\partial \boldsymbol{Y}} = \frac{1}{\boldsymbol{Le}} \nabla^2 \boldsymbol{S} \quad (3)$$

$$U = \frac{\partial \Psi}{\partial Y} \quad and \quad V = -\frac{\partial \Psi}{\partial X} \quad (4)$$

where Ψ, T, and S are the dimensionless stream function, temperature and concentration, respectively. U and V (X and Y) are the dimensionless horizontal and vertical velocities (coordinates).

Fig. 1. Schematic diagram of the physical problem.

The hydrodynamic, thermal and solutal boundary conditions associated with the present problem are:

$$\left. \begin{array}{l} For\ X = 0\ and\ 0 \leq Y \leq 1 : \Psi = 0, \dfrac{\partial T}{\partial X} = 0, S = 0 \\[2mm] For\ X = 1\ and\ 0 \leq Y \leq 1 : \Psi = 0, \dfrac{\partial T}{\partial X} = 0, S = 1 \\[2mm] For\ Y = 0\ and\ 0 \leq X \leq 1 : \Psi = 0, \dfrac{\partial S}{\partial Y} = 0, T = 1 \\[2mm] For\ Y = 1\ and\ 0 \leq X \leq 1 : \Psi = 0, \dfrac{\partial S}{\partial Y} = 0, T = 0 \end{array} \right\} \quad (5)$$

The above dimensionless equations show that the solutions for the present configuration are governed by five dimensionless parameters, namely, the thermal Rayleigh number R_T, the buoyancy ratio N, the Lewis number Le, the Hartmann number Ha and the normalized porosity ε. They are respectively defined as follow:

$$\left. \begin{array}{l} R_T = g \beta_T \Delta T' K L' / \alpha \nu \\[1mm] N = \beta_S \Delta S' / \beta_T \Delta T' \\[1mm] Le = \alpha / D \\[1mm] Ha = B_0 \sqrt{K \grave{o} / \mu} \\[1mm] \varepsilon = \varepsilon' / \sigma \end{array} \right\} \quad (6)$$

The normalized porosity and the Lewis number are fixed at $\varepsilon = 1$ and $Le = 10$ in the present study.

The heat and solute transfers across the cavity are given in terms of the Nusselt and Sherwood numbers defined as:

$$\left. \begin{array}{l} Nu = \displaystyle\int_0^1 \left. \frac{\partial T}{\partial Y} \right|_{Y=1} dX \\[4mm] Sh = \displaystyle\int_0^1 \left. \frac{\partial S}{\partial X} \right|_{X=0} dY \end{array} \right\} \quad (7)$$
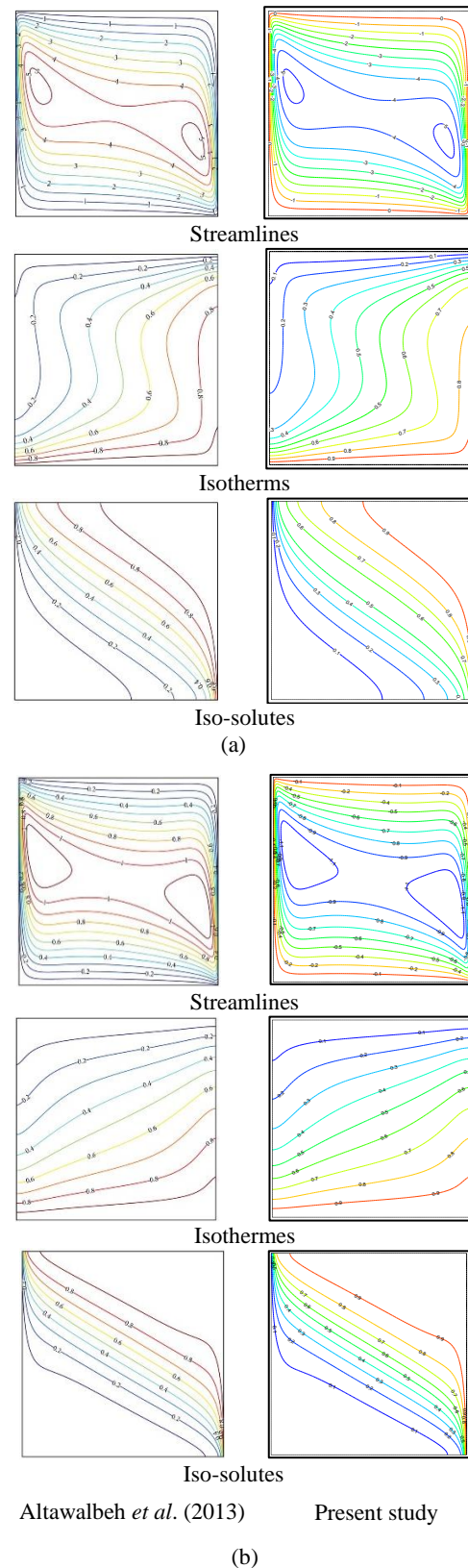
3. NUMERICAL MEHTOD

The governing equations are discretized using a central finite-difference scheme combined with the alternate direction implicit method (ADI). Details concerning the validation of the present code in the absence of the magnetic field were reported by Bourich *et al.* (2004). Its validity in the presence of a magnetic field was proved in the present study by comparing our results with those of Altawalbeh *et al.* (2013) as illustrated in Table 1.

Table 1 Validation of the numerical code for $R_T = 200$, $N = 1$, $Le = 10$ and various values of Ha.

		Ψ_{max}	Nu	Sh
$Ha=0$	Altawalbeh *et al.* (2013)	8.564	4.18	26.3
	Present study	8.438	4.062	24.53
	Deviation (%)	1.47	2.82	6.73
$Ha=1$	Altawalbeh *et al.* (2013)	5.328	3.293	25.458
	Present study	5.095	3.174	23.829
	Deviation (%)	4.37	3.61	6.4
$Ha=5$	Altawalbeh *et al.* (2013)	1.2	1.273	9.219
	Present study	1.177	1.267	8.990
	Deviation (%)	1.9	0.47	2.5

The comparison was performed in terms of Ψ_{max}, Nu and Sh for $R_T = 200$, $N = 1$, $Le = 10$ and three values of Ha (0, 1 and 5). The maximum deviation observed between our results and those of these authors is about 6.73%. The validation of the numerical code is reinforced by presenting also qualitative comparisons in terms of contour lines for $R_T = 200$, $Ha = 5$, $Le = 1$ and $N = 5$ (a) and $Le = 10$ and $N = 1$ (b). The comparative results presented in Figs. 2a-b show a good agreement between our results (on the right) and those of Altawalbeh *et al.* (2013) (on the left).

The effect of the grid size on the results corresponding to the monocellular, bicellular and tricellular flows obtained in this study was analyzed by using the uniform grids 61×61, 101×101 and 151×151. Tables 2 and 3 show that the characteristics of the flow and heat and mass transfer undergo negligible variations (lower than 0.4%) when the grid 101×101 is replaced by a finer grid 151×151. However, when the grid 61×61 is replaced by the grid 101×101 the results of Tables 2 and 3 show a maximum deviation of about 11% for Sherwood number. Based on these results, a grid of 101×101 nodes was adopted in the present study.

Streamlines

Isotherms

Iso-solutes

(a)

Streamlines

Isothermes

Iso-solutes

Altawalbeh *et al.* (2013)   Present study

(b)

Fig. 2. Comparison between our results and those of Altawalbeh *et al.* (2013) in terms of streamlines, isotherms and iso-solutes for $R_T = 200$, $Ha = 5$: $Le = 1$ and $N = 5$ (a) and $Le = 10$ and $N = 1$ (b).

Table 2 Effect of the Grid Size for $R_T = 1000$, $Le = 10$, $N = 0$ and Various Values of *Ha*.

Ha	Flow	Grids	$\left|\Psi_{ext}\right|$	*Nu*	*Sh*
0	TF	61×61	14.205	9.258	8.863
		101×101	13.93	9.151	9.966
		151×151	13.927	9.146	9.974
3	BNF	61×61	8.099	4.666	10.223
		101×101	8.110	4.648	10.679
		151×151	8.112	4.642	10.659
	TF	61×61	7.927	5.165	7.176
		101×101	7.903	5.156	7.550
		151×151	7.896	5.152	7.554

Table 3 Effect of the Grid Size for $R_T = 200$, $Le = 10$, $N = 0.2$ and Various Values of *Ha*.

Ha	Flow	Grids	$\left|\Psi_{ext}\right|$	*Nu*	*Sh*
0	MTF	61×61	9.148	4.027	15.930
		101×101	9.156	4.022	16.119
		151×151	9.159	4.020	16.056
2	BNF	61×61	2.665	1.924	11.839
		101×101	2.672	1.929	11.905
		151×151	2.674	1.931	11.876

4. RESULTS AND DISCUTION

The steady solutions submitted to the effect of a magnetic field in the present work are characterized by monocellular clockwise/trigonometric flow, bicellular natural/antinatural flow, and tricellular flow with a clockwise/trigonometric central cell and trigonometric/clockwise lateral cells, denoted MCF/MTF, BNF/BAF, and TCF/TTF, respectively. The streamlines (left), isotherms (middle) and iso-concentrations (right) corresponding to these solutions are illustrated in Figs. 3a-c for $R_T = 200$, $Le = 10$, $N = 0$ and $Ha = 0$. Other details about these solutions are available in the work by Mansour *et al.* (2006). Note that, for $N = 0$ (i.e. in the absence of solutal buoyancy forces), the intensities of the flow cells and the mean heat and mass transfer corresponding to MCF, TTF, and BNF are identical to those corresponding to MTF, TCF, and BAF, respectively.

The effect of the magnetic field and the multiplicity of solutions on the variations of *Nu* and *Sh* vs. R_T in the absence of solutal buoyancy forces is illustrated in Figs. 4a-c and Figs. 5a-c for $Le = 10$, $N = 0$ and $Ha = 0$, 1 and 3. Note that for $Ha = 0$, the monocellular (MF), bicelllular (BF) and tricellular (TF) flows were obtained for $R_T \geq 40$, $R_T \geq 80$ and $R_T \geq 160$, respectively. As expected, the increase of the Hartmann number retards the appearance of the different solutions. Hence, for $Ha = 1/(Ha = 3)$ the monocellular, bicelllular and tricellular flows were obtained for $R_T \geq 59/(R_T \geq 295)$, $R_T \geq 88/(R_T \geq 173)$ and $R_T \geq 197/(R_T \geq 270)$, respectively. Furthermore,


(a)

(b)

(c)
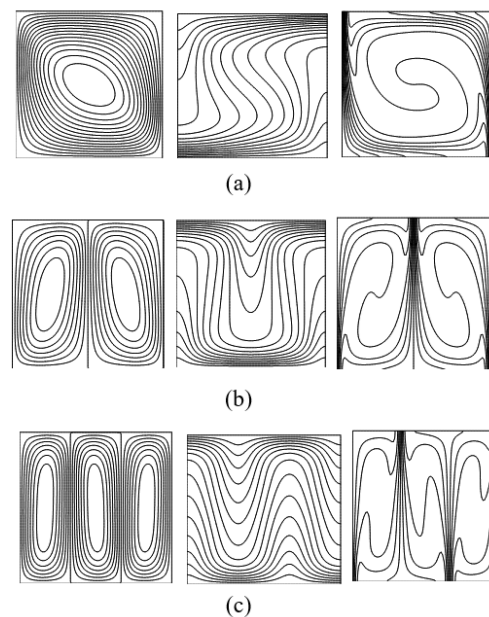
Fig. 3. Streamlines, isotherms and iso-solutes of monocellular flow (a), bicellular flow (b) and tricellular flow (c) obtained at $R_T = 200$, $Le = 10$, $N = 0$ and $Ha = 0$.
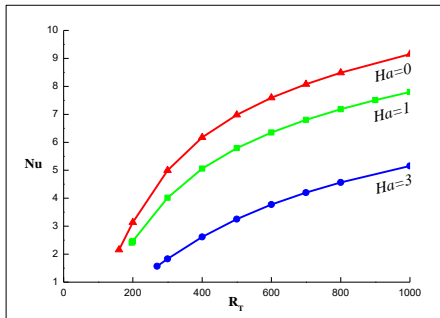
in the absence of the magnetic field, the transitions of the MF and BF toward oscillatory regimes occur at $R_T = 382$ and 710, respectively. For $Ha = 1$, these transitions are registered at $R_T = 445$ and 825. By increasing the Hartmann value to 3, the transition of the MF toward the oscillatory regime is delayed until
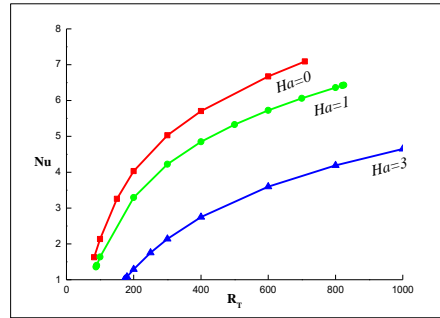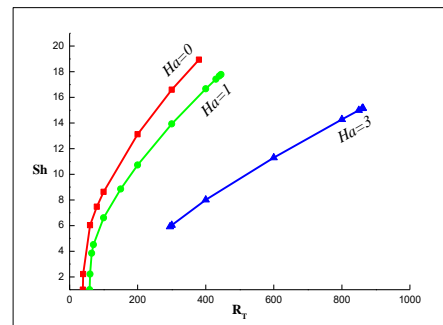
(a)
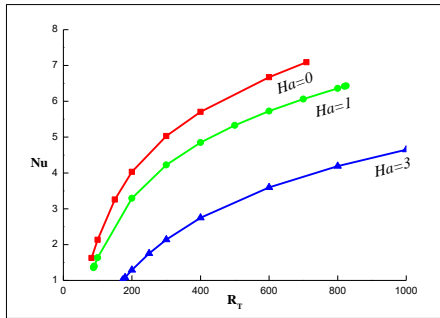
(b)

(c)

Fig. 4. Variations of Nu vs. R_T for $Le = 10$, $N = 0$ and various values of *Ha*: (a) monocellular flow, (b) bicellular flow and (c) tricellular flow.

$R_T = 862$, while the BF remains steady even for R_T exceeding 1000. Figures 4-5 show clearly that the increase of the magnetic field intensity reduces both heat and mass transfer rates. For example, at $R_T = 300$, by increasing *Ha* from 0 to 3, Nu/Sh decreases by about 64.5%/63.6%, 57.5%/46.8% and 63.4%/43.4% for the MF, the BF and the TF, respectively.

The effect of the multiplicity of solutions on the generated heat and mass transfers is illustrated in Figs. 6a-c and Figs. 7a-c where the evolutions of *Nu* and *Sh* vs. R_T are exemplified for the monocellular, bicelllular and tricellular flows in the cases of *Ha* = 0, 1 and 3. The arrows in these figures indicate the transitions undergone by each solution when R_T was progressively decreased starting from relatively large values of this parameter. It was observed that, for *Ha* = 0 and 1, the TF transits towards the BF at $R_T = 159$ and $R_T = 196$, respectively. The latter solution (BF)

transits toward the MF at $R_T = 81$ and 87 for *Ha* = 0 and 1, respectively. As it can be seen from these figures, the above transitions are accompanied with an increase in heat and mass transfer. For *Ha* = 3, both the MF and TF transit toward the BF at $R_T = 294$ and $R_T = 268$, respectively. The transition of the TF toward the BF induces an enhancement of *Nu* and *Sh* while the transition from the MF toward the BF enhances *Nu* but reduces *Sh*. In addition, the MF induces the weakest heat transfer in all its range of existence in the case of *Ha* = 3 (this is not the case for *Ha* = 0 and *Ha* = 1). Note also that, for *Ha* = 0 and 1, the rest state is reached through the MF (when R_T is progressively decreased), while for *Ha* = 3 the latter state is reached via the BF.
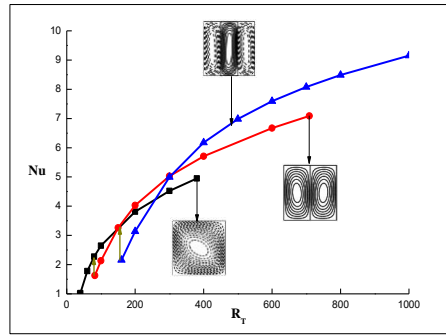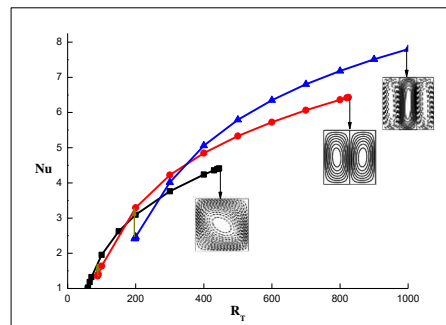

(a)
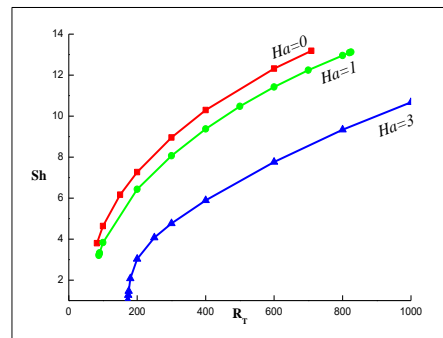
(b)
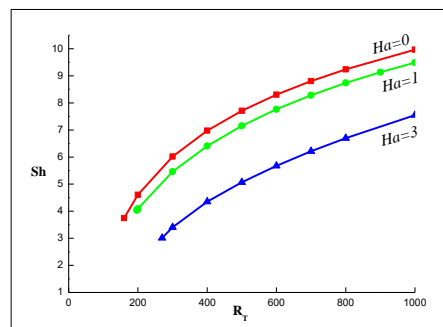
(c)

Fig. 5. Variations of Sh vs. R_T for $Le = 10$, $N = 0$ and various values of *Ha*: (a) monocellular flow, (b) bicellular flow and (c) tricellular flow.
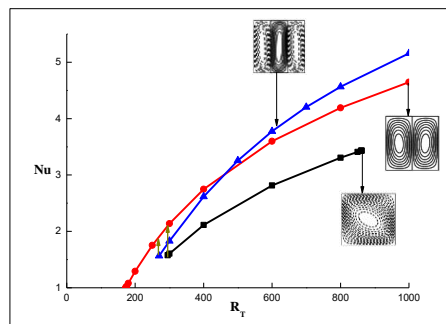
The effect of Hartmann number on the multiplicity of solutions and heat and mass transfer for $R_T = 200$,
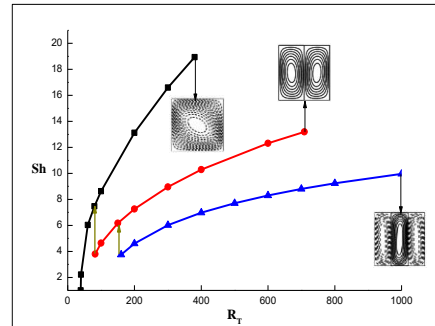
(a)

(b)

(c)

Fig. 6. Effect of R_T on Nu corresponding to monocellular, bicellular and tricellular flows for Le = 10, N = 0 and Ha = 0 (a), 1 (b) and 3 (c).

and mass transfers are controlled by pure diffusion (Nu = Sh = 1). It should be mentioned that within the existence range of these three steady solutions, the BF/MF induces the highest values of Nu/Sh, while the TF induces the weakest values for both Nu and Sh.

(a)

(b)

(c)

Fig. 7. Effect of R_T on Sh corresponding to monocellular, bicellular and tricellular flows for Le = 10, N = 0 and Ha = 0 (a), 1 (b) and 3 (c).

Table 4 Critical values of Ha corresponding to different transitions for R_T = 200, Le = 10 and N =0.

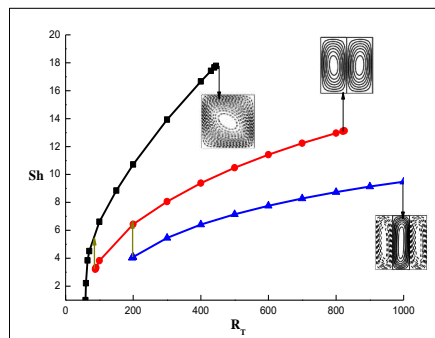| Flow mode	MCF	MTF	TCF	TTF
Transition toward	BNF	BAF	BAF	BNF
Ha_{cr}	2.445	2.445	1.067	1.067

Le = 10 and N = 0 is illustrated in Figs. 8a-b. These figures show that both the heat and mass transfer decrease by increasing the Hartmann number for all the flow modes considered. The arrows in these figures indicate the transitions obtained when Ha is progressively incremented from 0. The critical values of Ha corresponding to these transitions are given in Table 4.

The progressive increase of Ha from 0 leads to the transitions of the TF and MF toward the BF at $Ha_{cr} = 1.067$ and $Ha_{cr} = 2.445$, respectively. The first transition is accompanied by an enhancement of about 31.6 %/55.1% for Nu/Sh while the second transition leads to an increase of Nu by about 23.7% but to a decrease of Sh by about 18.9%. However, the BF is maintained until the critical value Ha_{cr} = 3.35, beyond which the flow vanishes and the heat
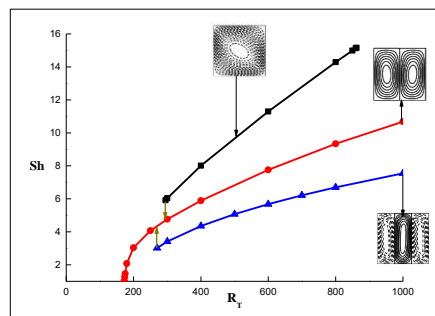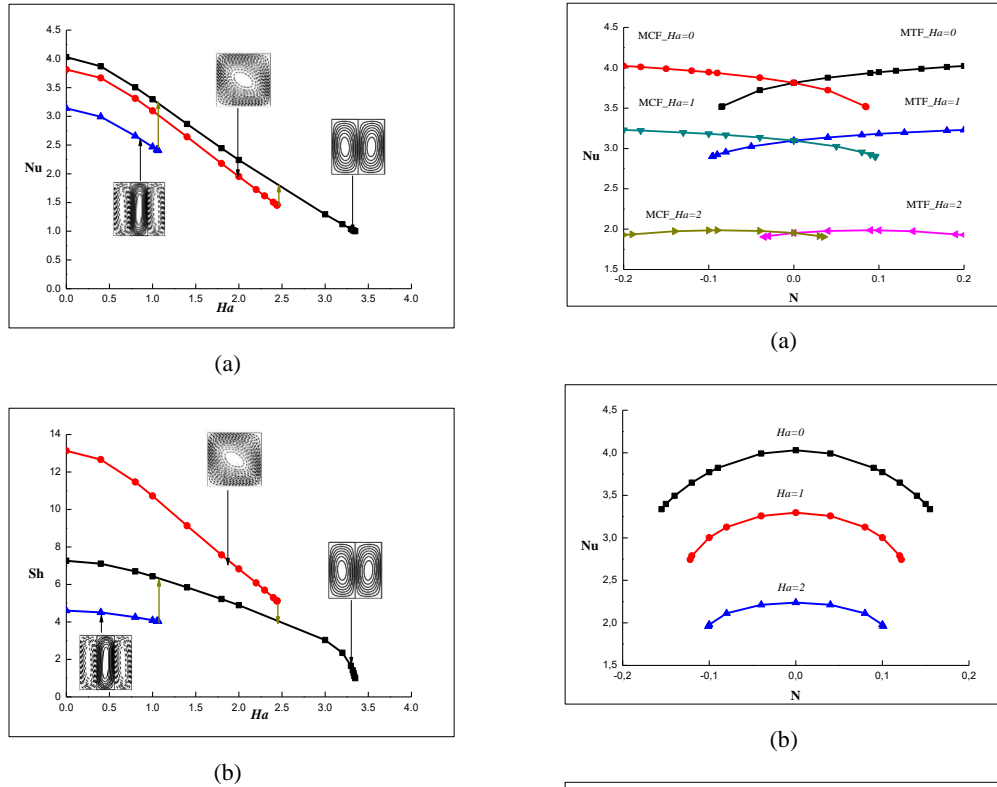
(a)

(b)

Fig. 8. Variations of *Nu* (a) and *Sh* (b) vs *Ha* for $R_T = 200$, $Le = 10$, $N = 0$ and different flow modes.

The aim of this section is to emphasize the magnetic field effect on the multiple steady state solutions obtained in the presence of solutal buoyancy forces ($N \neq 0$). Hence, Figs. 9-10 illustrate the evolutions vs. N (varying in the range $-0.2 < N < 0.2$) of Nu and Sh corresponding to moncellular (MTF and MCF), bicellular (BNF and BAF) and tricellular (TTF and TCF) flows for $R_T = 200$, $Le = 10$ and $Ha = 0$, 1 and 2. It should be mentioned that the tricellular flows were not obtained for $Ha = 2$ and $R_T = 200$. Note also that Nu and Sh corresponding to the MTF and TTF for $N > 0$ are identical respectively to those induced by the MCF and TCF for $N < 0$, whatever the Hartmann number value. In fact, the MTF/TTF and the MCF/TCF just exchange their roles while changing the sign of N. In addition, the BNF and the BAF induce identical average heat and mass transfers. Also, for the BF, the curves exemplifying the variations of Nu and Sh vs. N are symmetrical with respect to the vertical line passing through $N = 0$. Tables 5a-b summarize all the transitions observed and the corresponding critical values of N leading to these transitions. It can be seen from Figs. 9-10 that the increase of Ha reduces strongly the range of N corresponding to the tricellular mode. Moreover, Tables 5 indicate that the increase of Ha tends to reduce N_{cr} (in absolute value) corresponding to the transitions towards the MCF for $N < 0$ and the MTF for $N > 0$.
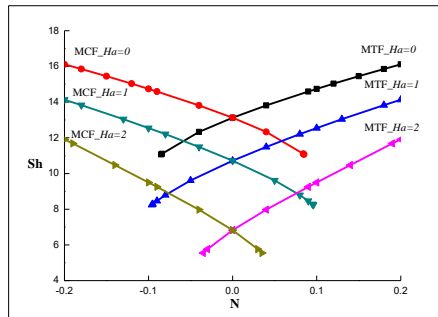

(a)

(b)

(c)
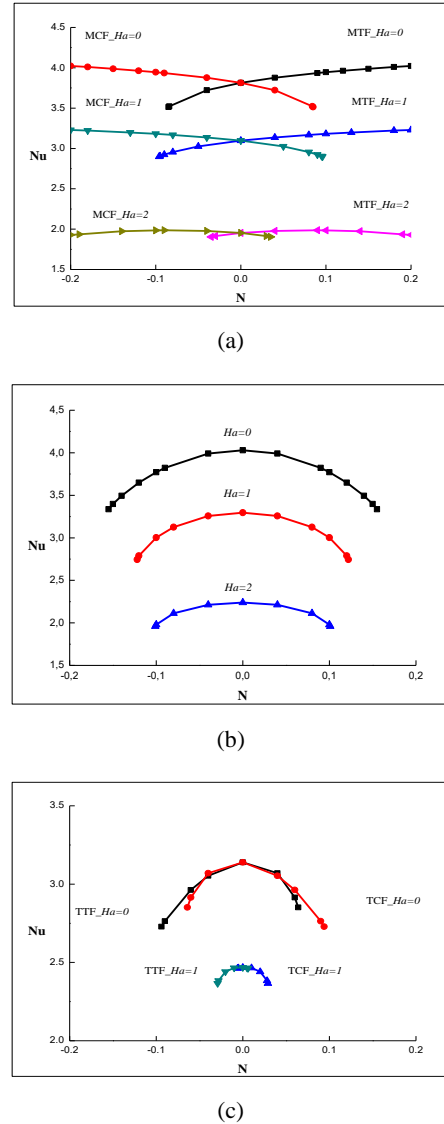
Fig. 9. Variations of *Nu* vs. *N* for $R_T = 200$, $Le = 10$ and different values of *Ha*: (a) MTF and MCF, (b) BF and (c) TTF and TCF

5   CONCLUSION

The influence of the magnetic field on the multiplicity of solutions induced by thermosolutal convection in a square porous cavity submitted to a destabilizing vertical gradient of temperature and to a horizontal concentration gradient was considered in this work. The effect of the Hartmann number on the maintaining and disappearance of the multiple steady-state solutions obtained in the case of pure thermal convection is examined. Based on the obtained results, the following findings are deduced:

- The presence of the magnetic field delays the transition towards the oscillatory regime when R_T is increased.
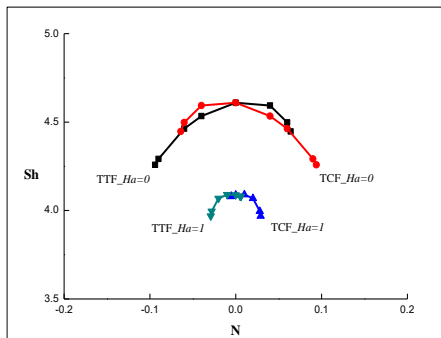
(a)
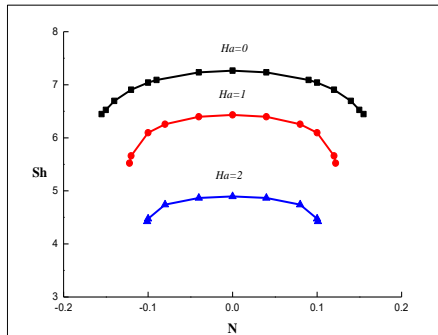
(b)

(c)

Fig. 10. Variations of *Sh* vs. *N* for $R_T = 200$, *Le* = 10 and different values of *Ha*: (a) MTF and MCF, (b) BF and (c) TTF and TCF.

The increase of *Ha* rises the critical Rayleigh number above which the different flow modes exist. Hence, $R_{T\_}$ rises from 40, 80 and 160 to 295, 173 and 270 when *Ha* is increased from 0 to 3 for the MF, BF and TF, respectively.

For *Ha* = 0 and 1, the TF transits towards the BF and the latter transits toward the MF, while for *Ha* = 3, both the MF and TF transit toward the BF, when R_T is decreased starting from a value that allows the existence of the three solutions.

For $R_T = 200$, *Le* = 10 and *N* = 0, the increase of *Ha* from 0 leads to the transitions of the TF and MF toward the BF at $Ha_{cr} = 1.067$ and $Ha_{cr} = 2.445$, respectively. The first transition is accompanied by an enhancement of 12.9 %

for *Nu* and 36.4% for *Sh*, while the second transition leads to an increase of *Nu* by 25.1% but to a decrease of *Sh* by 54%.

Tables 5 Transitions obtained for the different solutions and the corresponding critical values of *N* for $R_T = 200$, *Le* = 10 and *Ha* = 1, 1 and 2: (a) $N_{cr} > 0$ and (b) $N_{cr} < 0°$.

(a)

Flow mode	Transition towards	N_{cr}
Ha = 0		
MCF	BF	0.086
BF	MTF	0.156
TCF	MTF	0.065
TTF	BF	0.095
Ha = 1		
MCF	BF	0.097
BF	MTF	0.123
TCF	MTF	0.03
TTF	BF	0.007
Ha = 2		
MCF	BF	0.036
BF	MTF	0.102

(b)

Flow mode	Transition towards	N_{cr}
Ha = 0		
MTF	BF	-0.086
BF	MCF	-0.156
TCF	BF	-0.095
TTF	MCF	-0.065
Ha = 1		
MTF	BF	-0.097
BF	MCF	-0.123
TCF	BF	-0.007
TTF	MCF	-0.03
Ha = 2		
MTF	BF	-0.036
BF	MCF	-0.102

Finally, by examining the combined effects of the buoyancy ratio, *N*, and the Hartmann parameter, *Ha*, on the existence of different flow modes we concluded that:

The critical values of *N* corresponding to the transitions between the different solutions depend on the Hartmann number but the nature of the transitions remains unchanged.

The *Nu* and *Sh* corresponding to the MTF and TTF for *N* > 0 are respectively identical to those induced by the MCF and TCF for *N* < 0 regardless of the Hartmann number value. While the BNF and BAF induce identical average heat and mass transfers.

Generally, the increase of the magnetic field intensity reduces both heat and mass transfer rates for each flow mode.

REFERENCES

Ali, F. H., H. K. Hamzah, K. Egab, A. Müslüm and A. Shahsavar (2020). Non-Newtonian nanofluid natural convection in a U-shaped cavity under magnetic field. *International Journal of Mechanical Sciences.*186, 105887.

Altawalbeh, A., N. Saeid and I. Hashim (2013) Magnetic Field Effect on Natural Convection in a Porous Cavity Heating from below and Salting from Side. *Hindawi Publishing Corporation Advances in Mechanical Engineering. Article ID 183079, 13 pages*

Bahiraei, M. and M. Hangi (2015). Flow and heat transfer characteristics of magnetic nanofluids: A review. *Journal of Magnetism and Magnetic Materials* 374, 125-138.

Bourich, M., A. Amahmid and M. Hasnaoui (2004). Double diffusive convection in a porous enclosure submitted to cross gradients of temperature and concentration. *Energy Conversion and Management* 45, 1655-1670.

Chamkha, A. J. and H. Al-Naser (2002). Hydromagnetic double-diffusive convection in a rectangular enclosure with uniform side heat and mass fluxes and opposing temperature and concentration gradients. *International Journal of Thermal Sciences* 41, 936–948.

Chamkha, A. J. and H. Al-Naser (2002). Hydromagnetic double-diffusive convection in a rectangular enclosure with opposing temperature and concentration gradients. *International Journal of Heat and Mass Transfer* 45, 2465–2483.

Heidary, H., M. J. Kermani and M. Pirmohammadi (2016). Partition effect on thermo magnetic natural convection and entropy generation in inclined porous cavity. *Journal of Applied Fluid Mechanics* 9, 119-130.

Hoshyar, H. A., D. D. Ganji and A. R. Majidian (2016). Least square method for porous fin in the presence of uniform magnetic field. *Journal of Applied Fluid Mechanics* 9, 661-668.

Hussein, A., H. Ashorynejad, M. Shikholeslami and S. Sivasankaran (2014). Lattice Boltzmann simulation of natural convection heat transfer in an open enclosure filled with Cu-water nanofluid in a presence of magnetic field. *Nuclear Engineering and Design* 268, 10-17.

Kabeel, A. E., Emad M. S. El-Said and S. A. Dafea (2015). A review of magnetic field effects on flow and heat transfer in liquids: Present status and future potential for studies and applications. *Renewable and Sustainable Energy Reviews* 25, 830-837.

Kasaeian, A., R. D. Azarian, O. Mahian, L. Kolsi, A. J. Chamkha, S. Wongwises and I. Pop g (2017). Nanofluid flow and heat transfer in porous media: A review of the latest developments. *International Journal of Heat and Mass Transfer* 107, 778–791.

Krakov, M. S. and I. V. Nikiforov (2002). To the influence of uniform magnetic field on thermomagnetic convection in square cavity.

Journal of Magnetism and Magnetic Materials 252, 209–211.

Maatki, C., L. Kolsi, H. F. Oztop, A. Chamkha, M. N. Borjini, H. Ben Aissia and K. Al-Salem (2013). Effects of magnetic field on 3D double diffusive convection in a cubic cavity filled with a binary mixture. *International Communications in Heat and Mass Transfer* 49, 86–95.

Mansour, A., A. Amahmid, M. Hasnaoui and M. Bourich (2006). Multiplicity of solutions induced by thermosolutal convection in a square porous cavity heated from below and submitted to horizontal concentration gradient in the presence of Soret effect. *Numerical Heat Transfer* Part A, 49, 69-94.

Nanjundappa, C. E., I. S. Shivakumara and H. N. Prakash (2012). Penetrative ferroconvection via internal heating in a saturated porous layer with constant heat flux at the lower boundary. *Journal of Magnetism and Magnetic Materials* 324, 1670–1678.

Ramambason Rakoto, D. S. and P. Vasseur (2007). Influence of a magnetic field on natural convection in a shallow porous enclosure saturated with a binary fluid. *Acta Mechanical* 191, 21–35.

Robillard, L., A. Bahloul and P. Vasseur (2006). Hydromagnetic natural convection of a binary fluid in a vertical porous enclosure. *Chemical Engineering Communications* 193, 1431-1444.

Sheikhnejad, Y., R. Hosseini and M. S. Avval (2017). Experimental study on heat transfer enhancement of laminar ferrofluid flow in horizontal tube partially filled porous media under fixed parallel magnet bars. *Journal of Magnetism and Magnetic Materials* 424, 16-25.

Sophy, T., H. Sadat and L. Gbahoue (2005). Convection thermomagnétique dans une cavité différentialement chauffée. *International Communications in Heat and Mass Transfer* 32, 923–930.

Teamah, M. A. and A. I. Shehata (2016). Magnetohydrodynamic double diffusive natural convection in trapezoidal cavities. *Alexandria Engineering Journal* 55, 1037-1046.

Teamah, M. A., A. F. Elsafty and E. Z. Massoud (2012). Numerical simulation of double-diffusive natural convective flow in an inclined rectangular enclosure in the presence of magnetic field and heat source. *International Journal of Thermal Sciences* 52, 161-175.

Zeng, M., Q. W. Wang, Z. P. Huang, G. Wang and H. Ozoe (2007). Numerical investigation of natural convection in an enclosure filled with porous medium under magnetic field. *Numerical Heat Transfer, Part A* 52, 959-971.